Oscillatory temporal behavior in an autocatalytic surface reaction model

J.-P. Hovi, A. P. J. Jansen,* and R. M. Nieminen
Laboratory of Physics, Helsinki University of Technology, 02150 Espoo, Finland
(Received 11 November 1996)

We discuss an autocatalytic surface reaction model $A+B\rightarrow 2B$, where particle A (B) adsorbs (desorbs) the surface with rate constant ζ $(1-\zeta)$. We present numerical results from Monte Carlo simulations in dimensions $d=1$, 2, and 3, as well as some analytical results, which are valid in any dimension. Especially the static aspects of this model, like the behavior of the average coverages as a function of the control parameter ζ, are well understood from simple arguments which use the rate equations. Numerical studies of the temporal behavior of this model reveal periodic oscillations in the coverages for $d=2$ and 3, but not for $d=1$. Our data show that these periodic oscillations are related to *synchronized* avalanches of autocatalytic reactions. These avalanches occur with a well defined frequency, and come in *all* possible sizes. To explain this effect we give a heuristic argument, which postulates that the model is driven toward a critical state of a random deposition problem. [S1063-651X(97)13603-0]

PACS number(s): 68.10.Jy, 82.20.Wt, 82.65.Jv

I. INTRODUCTION

Heterogenous catalytic reactions far from thermal equilibrium are of great interest for practical applications as well as from a fundamental standpoint. In particular, these reactions may exhibit many kinds of nonlinear phenomena, like periodic behavior in several length or time scales [1,2]. Well studied examples of surface reactions with such temporal and spatial oscillations include CO oxidation on Pt-group metals [3–5], NO-CO reaction on Pt and Pd [6–8], and oxidation of H_2 on Pt [9,10].

Although it is well established that these oscillations arise from nonlinearities within the reaction, there may be several possible mechanisms that cause the effect. For example, the oscillations in CO oxidation on Pt surfaces at low pressures have been associated with adsorbate-induced transformation of the surface structure [3]. At higher pressures the dominant mechanism appears to be the oxide formation [11]. Pd(110) shows oscillations in CO oxidation as well as period doubling, presumably due to subsurface adsorption of oxygen [12]. Another experiment on Pd revealed none of the spatial structures observed for CO on Pt, possibly because of the homogenizing effect of gas-phase coupling [13]. Thus the possible feedback mechanisms responsible for the oscillatory behavior come in many different forms indeed.

Understanding these mechanisms poses a major challenge for modern surface science studies. In this respect simple models play an important role by allowing one to investigate the mechanisms in great detail. They also serve as a basis toward more realistic simulations of reaction systems. Often the models are defined in terms of stochastic rules, which describe how the system evolves from one configuration to another. The rules simulate different reaction steps, such as adsorption, reaction, or desorption, hence capturing some of the essential features of large classes of reaction systems. The correct time scale for the evolution can be achieved by considering the master equation of the system [14–16].

In this paper we investigate a simple autocatalytic surface reaction model, which produces temporal oscillations in the particle densities [17]. This model consists of two kinds of particles, say, A and B. Particle A adsorbs with rate ζ, particle B desorbs with rate $1-\zeta$, and there is an infinitely fast autocatalytic reaction step $A+B\rightarrow 2B$ occurring on the surface (see Sec. II). This results in a simple model whose behavior depends only on a single parameter ζ.

The model has been studied in two dimensions (2D) by Mai, Kuzovkov, and von Niessen [17], who used it in testing the applicability of different approximations (such as the mean field approximation) in the context of a spatially correlated system. In fact, even quite complicated approximations, such as their ''correlation analysis'' [18], seem to fail in the description of this reaction system. For example, Mai, Kuzovkov, and von Niessen concluded that there exists a ''critical'' $\tilde{\zeta}\approx 0.11$ below which the particle densities oscillate in time. They also argued that the origin of the oscillations is the instability between a reactive, i.e., a state with nonzero density of B particles, and A-poisoned phases of the system. Our findings do not support these conclusions.

In this paper we concentrate on the complicated temporal behavior of the model. In particular, we study the origin of the periodic oscillations. We present numerical results from Monte Carlo simulations carried out in dimensions $d=1$, 2, and 3, as well as some interesting analytical results, which are valid for any dimension. Average quantities, like the average number of B molecules, are well understood from these simple analytical results. In addition, we find oscillations, near $\zeta=0$, for $d=2$ and 3, but not for the 1D model. Our data show that these periodic oscillations are related to *synchronized* avalanches of $A+B\rightarrow 2B$ reactions. These avalanches occur with a well defined frequency, and come in *all possible sizes*. We do not have a complete theory for the emergence of the oscillations, but we give a simple heuristic argument (different from that of Ref. [17]), which postulates that the model is driven toward a critical state of a random

*Permanent address: Laboratory of Inorganic Chemistry and Catalysis, Eindhoven University of Technology, 5600 MB Eindhoven, The Netherlands.

deposition problem. This heuristics is qualitatively able to account for the observed temporal behavior of this model in $d \leqslant 3$.

The rest of this paper is organized as follows. We introduce the model in Sec. II, which is followed by a discussion of our analytical results (Sec. III). In particular, our analytical results enable us to introduce a method, the constant-B coverage ensemble, to study the problem for very small ζ. These simulation algorithms, including the constant-B coverage ensemble similar to that introduced in Ref. [19], are discussed in Sec. IV. In Sec. V we report results from computer simulations in $d=1$, 2, and 3 hypercubic lattices with periodic boundaries. The discussion, Sec. VI, contains a brief account of the static aspects of the model (Sec. VI A), as well as the possible heuristic explanation for the emergence of these oscillations (see Sec. VI B). A short conclusion completes the paper in Sec. VII.

II. MODEL DESCRIPTION

The model consists of two kinds of particles, denoted A and B, which follow the reaction sequence

$$A+*\overset{\zeta}{\rightarrow}A*, \tag{1}$$

$$B*\overset{1-\zeta}{\rightarrow}B+*, \tag{2}$$

$$A*+B*\overset{\infty}{\rightarrow}2B*, \tag{3}$$

where the asterisk denotes a vacant site, and superscript asterisk stands for an adsorbed particle. With sufficient generality the catalysis surface can be simulated by a d-dimensional hypercubic lattice, where the autocatalytic reaction step occurs only between nearest-neighbor particles on that lattice. It is also convenient to scale time so that the rate constant of the A adsorption equals ζ, and of B desorption $1-\zeta$, while the last autocatalytic step is infinitely fast. Thus the whole reaction sequence Eqs. (1)–(3) depends only on a single parameter ζ. The rate constants are transition probabilities in the master equation for the system [16].

This model has several potential experimental realizations in $d=2$, simulating a class of possible realistic feedback mechanisms. For example, A and B could be the same molecule, which are adsorbed differently. Then A may denote a chemisorbed and B a physisorbed molecule, as neighboring B weakens the bonding of A and turns it to B [see Eq. (3)]. Alternatively, B may be adsorbed on a reconstructed site, and such a molecule induces the same reconstruction on a neighboring unreconstructed occupied site. On the other hand, A could be B plus an additional ligand. Such a ligand could desorb immediately if A and B come into contact, leaving two B's on the surface. We may also think of a forest fire model: let A denote a green, and B a burning tree. In particular, for small ζ the trees grow slowly and burn fast.

III. ANALYTICAL RESULTS

It is convenient to characterize the macroscopic state of the system by monitoring the coverages $\theta_i(t)$, $(i=*,A,B)$, i.e., the fraction of sites occupied by particle i at the time t. Because every site is either vacant or occupied by A or B, these coverages obey a conservation law

$$\theta_A(t)+\theta_B(t)+\theta_*(t)=1. \tag{4}$$

It is easy to write the time evolution of the coverage in the form of rate equations

$$\frac{d\theta_A}{dt}=\zeta\theta_*-zK[AB], \tag{5}$$

$$\frac{d\theta_B}{dt}=-(1-\zeta)\theta_B+zK[AB], \tag{6}$$

$$\frac{d\theta_*}{dt}=-\zeta\theta_*+(1-\zeta)\theta_B, \tag{7}$$

where $[AB]$ is the probability to find a B to the right of an A at an arbitrary horizontal pair of neighboring sites, and the factor $z=2d$ follows from the use of square symmetry, e.g., $[AB]=[BA]$, in d dimensions. The parameter K is the rate constant of the autocatalytic reaction. Note that although we are interested in the infinitely fast reaction rate $K\rightarrow\infty$, the product $K[AB]$ may remain finite. Equations (5), (6), and (7) are exact, but contain the distribution $[AB]$, which is unknown.

Some time averaged results for the coverages can be derived, because the time average of the derivatives at the left hand side of Eqs. (5), (6), and (7) vanish. In that case Eq. (7) gives

$$\zeta\langle\theta_*\rangle=(1-\zeta)\langle\theta_B\rangle, \tag{8}$$

where the brackets denote the time averaging. Equation (8) simply states that on average the number of adsorbing A's must equal the number of desorbing B's. In addition, using Eqs. (4) and (8), we find that the average coverage of one species is enough to determine the coverages of other species, e.g.,

$$\langle\theta_B\rangle=\frac{\zeta}{1-\zeta}\langle\theta_*\rangle=\zeta(1-\langle\theta_A\rangle). \tag{9}$$

This *exact* relation is an important guide to study the model in the limit $\zeta\rightarrow 0$ (see Sec. IV).

It is easy to solve Eqs. (5), (6), and (7) in the mean field approximation (MFA), which involves setting $[AB]=\theta_A\theta_B$. A straightforward calculation yields equilibrium points $(\langle\theta_A\rangle,\langle\theta_B\rangle)=(1,0)$ and $(\zeta/zK,\zeta-\zeta^2/zK)$ [17]. The A-poisoned state corresponds to a saddle point, so the system will evolve to $(\zeta/zK,\zeta-\zeta^2/zK)\rightarrow(0,\zeta)$, as $K\rightarrow\infty$. Previous work [17,20] has clearly pointed out that the MFA is inadequate to describe the behavior of this model, as it fails to predict the temporal oscillations of the coverages (see Sec. V B). However, it is interesting to note that the MFA gives

$$\langle\theta_B\rangle=\zeta^{\beta_{\mathrm{MF}}+1}, \tag{10}$$

$$1-\langle\theta_A\rangle=1=\zeta^{\beta_{\mathrm{MF}}}, \tag{11}$$

with $\beta_{\mathrm{MF}}=0$. Below, we shall compare this prediction with numerical data.

Another useful observable is the average number of $A+B\rightarrow 2B$ reactions per A adsorption,

$$\overline{s_{\mathrm{ads}}}(\zeta)=\sum_{s=0}^{\infty} sP_{\mathrm{ads}}(s,\zeta), \tag{12}$$

where $P_{\mathrm{ads}}(s,\zeta)$ is the probability that an adsorption of A is immediately followed by s autocatalytic reactions [see Eq. (3)] for given ζ. If A adsorbs on a site without neighboring $B, s=0$. Because at the steady state each adsorbing A will later transform into B via the autocatalytic reaction, we have the constraint $\overline{s_{\mathrm{ads}}}=1$ for all ζ. Thus it is more interesting to look only at real *avalanches*; i.e., the distribution of the number of A's which turn into B's following an A adsorption. The average size $\overline{s}$ of these avalanches is given by

$$\overline{s(\zeta)}=\sum_{s=1}^{\infty} sP(s,\zeta), \tag{13}$$

where $P(s,\zeta)$ is the probability that an avalanche has size s. In other words, $P(s,\zeta)$ is the size distribution of A clusters on the surface, and $\overline{s(\zeta)}$ is the mean cluster size. Distribution $P(s,\zeta)$ is proportional to $P_{\mathrm{ads}}(s,\zeta)$ for $s\geqslant 1$. The proportionality constant can be derived from the normalization. We have $\Sigma_{s=0}^{\infty}P_{\mathrm{ads}}(s,\zeta)=\Sigma_{s=1}^{\infty}P(s,\zeta)=1$, which leads to

$$P(s,\zeta)=\frac{P_{\mathrm{ads}}(s,\zeta)}{1-P_{\mathrm{ads}}(0,\zeta)}. \tag{14}$$

Consequently,

$$\overline{s}=\frac{1}{1-P_{\mathrm{ads}}(0,\zeta)}. \tag{15}$$

In the spirit of the MF approximation we may assume that, if ζ is small, θ_B is small as well, and therefore all B's are well separated

$$P_{\mathrm{ads}}(0,\zeta)\approx\frac{\langle\theta_*\rangle-z\langle\theta_B\rangle}{\langle\theta_*\rangle}. \tag{16}$$

In that case

$$\overline{s(\zeta)}\approx\frac{\langle\theta_*\rangle}{z\langle\theta_B\rangle}=\frac{1-\zeta}{z\zeta}, \tag{17}$$

where the last step follows from Eq. (8). This approximate calculation gives a solid reason to anticipate that the size of the avalanches, i.e., the mean size of A clusters, diverges as $\zeta\rightarrow 0$. Such a divergence dictates that we expect the model to possess a critical point $\zeta_c=0$ (for all d), and

$$P(s,0)\propto s^{-\tau}\quad\text{for } s\gg 1, \tag{18}$$

with $\tau\leqslant 2$.

IV. NUMERICAL METHODS

We have performed Monte Carlo simulations in d-dimensional hypercubic lattices with $d=1$, 2, and 3 using periodic boundary conditions. We utilize two kinds of simulations, which are described below.

A. Direct Monte Carlo simulations

These simulations were started from a lattice fully covered with B's at time $t=0$. Subsequently we followed the time evolution of the system according to Eqs. (1), (2), and (3). The correct time scale for the evolution of the system was obtained by considering the transition probabilities $W_{\beta\alpha}$, which indicate the probability for the system to evolve from a configuration α to β. (These transition probabilities are ζ for A adsorption, $1-\zeta$ for B desorption, and K for the autocatalytic reaction.) In particular, the first reaction which brings the system from α to β will take time Δt, which is exponentially distributed [14–16],

$$\Delta t=-\frac{1}{R_\alpha}\ln r, \tag{19}$$

where $R_\alpha=\Sigma_\beta W_{\beta\alpha}$ is the total transition rate from the configuration α, and r is a uniformly distributed random number, $0<r<1$. Specifically, using Eqs. (1), (2), and (3),

$$R_\alpha(t)=N_B(1-\zeta)+N_*\zeta, \tag{20}$$

where $N_B(N_*)$ is the number of B molecules (vacant sites) at time t. The first term in Eq. (20) indicates the probability of B desorption, and the second of A adsorption. The infinitely fast $A+B$ reactions do not affect Δt.

Thus the simulation algorithm is the following:

(1) Calculate R_α from Eq. (20). Update the clock $t\rightarrow t+\Delta t$ [see Eq. (19)].

(2) With the probability $N_*\zeta/R_\alpha$ the next reaction is A adsorption, otherwise B desorption.

(3) If the next reaction is B desorption, then randomly select a site which is occupied by a B and make it empty. Update $N_*\rightarrow N_*+1$, $N_B\rightarrow N_B-1$, and go to 1.

(4) If the next reaction is A adsorption, then select a vacant site at random and fill that with A. Update $N_*\rightarrow N_*-1$.

(5) Check the nearest-neighbor sites.

(6) If there are no B next to the newly adsorbed A, then go to (1).

(7) Identify all s A's which belong to the same cluster with the newly adsorbed A. Turn them into B's. Update $N_B\rightarrow N_B+s$. Go to (1).

The system was simulated for $(2–15)\times 10^3$ time units. The first half of the time steps were discarded in order to allow the system to evolve into a steady state. During the latter half of the simulation we monitored the time evolution of the coverages of the adsorbates, as well as collected histogram of the probability distribution of the avalanche sizes s.

We simulated system sizes between 10^6 and 2×10^7 sites. Because the fluctuations in the coverages, which may drive a finite system to the A poisoned state, are larger for smaller ζ (see below), we increased the system size gradually as $\zeta\rightarrow 0$. However, due to the larger fluctuations and limitations in the available computer memory, we could not simulate the system behavior properly for very small ζ. To this end we utilized another simulation method, the constant-B coverage ensemble, which is described below.

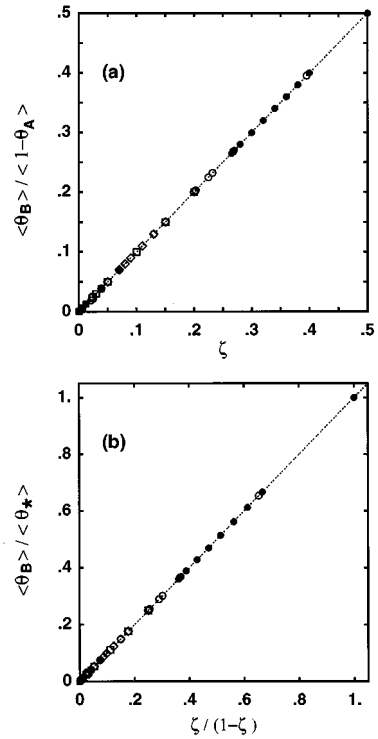

FIG. 1. The ratio (a) $\langle\theta_B\rangle/(1-\langle\theta_A\rangle)$ vs ζ, and (b) $\langle\theta_B\rangle/\langle\theta_*\rangle$ vs $\zeta/(1-\zeta)$. The data are collected using both direct simulations (filled markers) and constant-B coverage ensemble (open markers). Different symbols denote the results from 1D (○), 2D (◇), and 3D (□) hypercubic lattices. The dashed lines on the diagonal are Eq. (9).

B. Simulations with constant-B coverage

This approach is based on Eq. (9), which implies that the average coverage of two species can be used to determine ζ, e.g.,

$$\zeta=\frac{\langle\theta_B\rangle}{(1-\langle\theta_A\rangle)}. \tag{21}$$

We started the simulations from a system where a fixed fraction of sites, the target B coverage θ_B, was randomly occupied by B's, while the rest of the sites were empty. Subsequently the system was simulated similarly to Sec. IV A, but the choice between B desorption and A adsorption was determined by the B coverage at time t. If $\theta_B(t)>\theta_B$, the next reaction was B desorption, otherwise A adsorption. In this manner $\theta_B(t)$ was kept at the target coverage θ_B on average. After a certain transient period the system evolved to a steady state, and the average coverage of A's, θ_A, was measured. Using Eq. (21) we can determine the effective value of ζ which corresponds to these values of θ_A and θ_B.

This method facilitates the simulations at small ζ. In practice, the lower limit in ζ is dictated by the available computer memory, because we require $N_B\gg 1$, i.e., θ_B cannot be too small. In this work we performed simulations down to $\theta_B=10^{-4}$–10^{-3}, which corresponds to $\zeta\approx 10^{-4}$–10^{-3}.

On the other hand, because the time evolution of the system was not determined by the master equation, these simulations do not have the correct time dependence. Therefore we could not use this method for studying the dynamical behavior of the system, but only average coverages as well as the avalanche size distribution were monitored. In principle, lack of the correct time dependence could also mean that the measured θ_A differs from the true time averaged value $\langle\theta_A\rangle$. We studied this by measuring $\langle\theta_A\rangle$ and $\langle\theta_B\rangle$ from direct Monte Carlo (MC) simulations, and performing a constant-B coverage simulation at $\theta_B=\langle\theta_B\rangle$. Within the numerical accuracy we found that the A coverages of these two simulation methods coincided, $\theta_A=\langle\theta_A\rangle$.

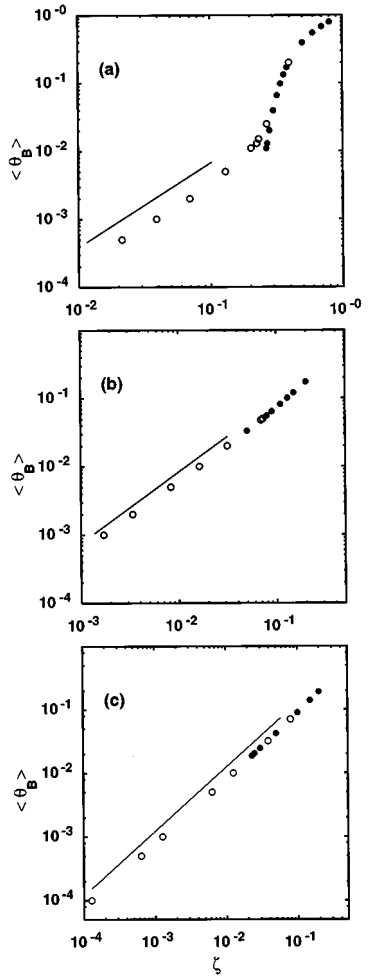

FIG. 2. The log-log plot of $\langle\theta_B\rangle$ as a function of ζ from (a) 1D, (b) 2D, and (c) 3D hypercubic lattices. The data are collected using both direct simulations (●) and a constant-B coverage ensemble (○). The solid lines, which depict the power-law behavior for small ζ, have slopes (a) 1.24, (b) 1.04, and (c) 1.01.

V. SIMULATION RESULTS

A. Average coverages

In this section we study the average coverages as a function of ζ. We start by checking Eq. (9), which suggests that it is sufficient to monitor only the coverage of one species of adsorbants, for example, $\langle\theta_B\rangle$. Figure 1 shows the ratios $\langle\theta_B\rangle/(1-\langle\theta_A\rangle)=\zeta$ and $\langle\theta_B\rangle/\langle\theta_*\rangle=\zeta/(1-\zeta)$ for $d=1$, 2, and 3 hypercubic lattices. The data are collected using both direct and constant-B coverage simulations. Indeed, all the

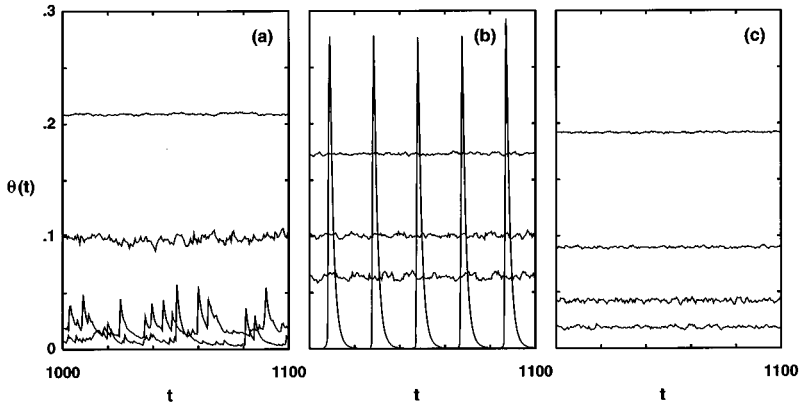

FIG. 3. $\theta_B(t)$ for (a) 1D, (b) 2D, and (c) 3D hypercubic lattices. Each panel displays typical simulation results for four values of ζ (from top to bottom): (a) $\zeta=0.40$, 0.34, 0.28, and 0.265; (b) $\zeta=0.20$, 0.13, 0.09, and 0.05; and (c) $\zeta=0.20$, 0.10, 0.05, and 0.023.

data collapse excellently on the diagonal lines of Fig. 1 [see Eq. (9)], independent of the dimensionality. This also numerically justifies the constant-B ensemble, which we have used especially for small ζ.

Figure 2 shows $\langle\theta_B\rangle$ as a function of ζ for the hypercubic lattices using both direct and constant-B coverage simulations. For clarity, the figure does not show overlapping points, but it can be seen that the data from both ensembles again fall on the same curve, except for some deviations in Fig. 2(a) at $\zeta\approx0.27$. The constant-B-coverage simulation does not give the same result as the direct one in 1D, because the former method forces the system into the reactive state even when the system would like to poison for $\xi<0.265$. In fact, direct simulations in 1D for $\zeta<0.265$ always tend towards an A-poisoned state due to the finite system sizes which we could simulate. More accurate computations with constant-B ensemble numerically confirm that there exists a reactive steady state for all $\zeta>\zeta_c=0$, as discussed below Eq. (17).

Figure 2 also shows that $\langle\theta_B\rangle$ is quite a complicated function of ζ, especially in 1D. The data for $\langle\theta_A\rangle$ and $\langle\theta_*\rangle$ also show similar behavior (data not shown). However, for small ζ, i.e., near ζ_c, all the data seem to approach a power law (see, e.g., the solid lines in Fig. 2)

$$\langle\theta_B\rangle\propto\zeta^{\beta+1}, \tag{22}$$

$$1-\langle\theta_A\rangle=\zeta^{-1}\langle\theta_B\rangle\propto\zeta^{\beta}, \tag{23}$$

$$\langle\theta_*\rangle=\frac{1-\zeta}{\zeta}\langle\theta_B\rangle\propto\zeta^{\beta}. \tag{24}$$

Using least square fits to the data of Fig. 2, we find $\beta_{1D}=0.24\pm0.04$, $\beta_{2D}=0.04\pm0.04$, and $\beta_{3D}=0.01\pm0.04$. Similar analysis of the data for $\langle\theta_A\rangle$ and $\langle\theta_*\rangle$ gave consistent results, although the corrections to the asymptotic behavior seem to be more important in these data than for $\langle\theta_B\rangle$. The above error bars of β are dominated by the spread of the fits depending on which set of the data was used in the analysis.

We can now compare the above measurements with the MFA results, Eqs. (10) and (11), where $\beta_{MF}=0$. We find that $\langle\theta_B\rangle$ and $1-\langle\theta_A\rangle$ behave as in Eqs. (10) and (11) sufficiently close to ζ_c. In particular, in 2D and 3D the data are consistent with $\beta_{2D}=\beta_{3D}=0$. However, β_{1D} is clearly different from zero. In other words, our simulations indicate that in 1D $\lim_{\zeta\to0}(\theta_A,\theta_B,\theta_*)=(1,0,0)$, but in higher dimensions the steady state approaches to a mixture of A particles and vacant sites.

B. Coverages as a function of time

The main motivation for studying this particular model is the complicated temporal behavior, involving periodic oscillations in the coverages. Because the constant-B coverage ensemble lacks the correct time dependence, all the results of this section are from direct MC simulations. Unfortunately, this excludes the simulations for very small ζ.

Figure 3 displays the temporal evolution of $\theta_B(t)$ for several values of ζ. It can be seen that the amplitude of fluctuations increases with decreasing ζ. This behavior is most clearly seen in 2D data of Fig. 3(b), where especially the data for $\zeta=0.05$ show clear oscillatory behavior.

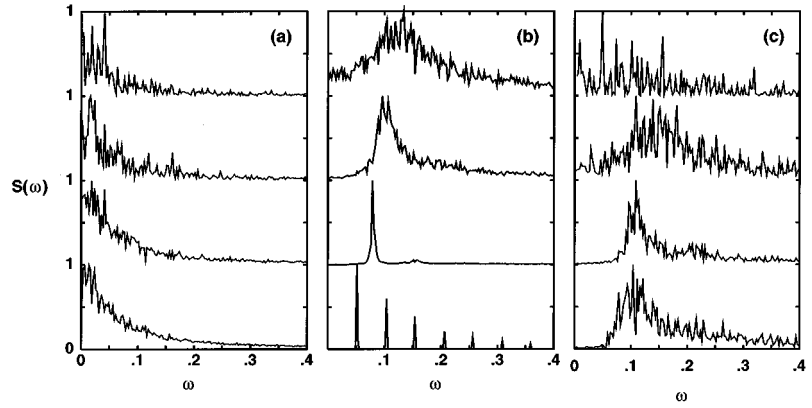

FIG. 4. The power spectra $S(\omega)$ of the Fourier-transforms of the data of Fig. 3. Panels show $S(\omega)$ for (a) 1D, (b) 2D, and (c) 3D hypercubic lattices, with the same values of ζ as in Fig. 3 (ζ decreases from top to bottom). For clarity, raw $S(\omega)$ is normalized such that the maximum equals unity.

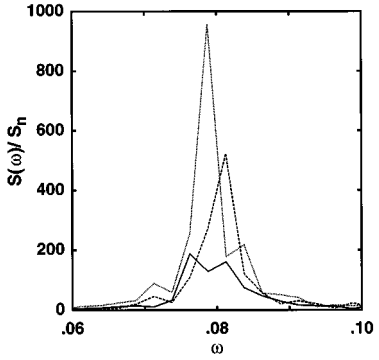

FIG. 5. The scaled power spectrum $S(\omega)/S_n$, which describes the signal to noise ratio, for different system sizes L: solid, dashed, and dotted lines show the data for $L=512$, 1024, and 2000, respectively. Data are from 2D simulations at $\zeta=0.09$.

To analyze these oscillations in more detail, we Fourier transformed the data of Fig. 3. Resulting power spectra $S(\omega)$ are shown in Fig. 4. For clarity, the S's are normalized such that the maximum equals unity. We find that especially the spectra of 2D and 3D data in Figs. 4(b) and 4(c) show clear peaks, i.e., fingerprints of periodic oscillations in $\theta_B(t)$, with a well defined frequency ω. The oscillations are again especially clear in the spectrum of 2D data with $\zeta=0.05$, where we can distinguish more than ten overtones (only six of them are shown in Fig. 4). The peaks of 2D and 3D spectra become more and more pronounced as $\zeta\to 0$, which again indicates that the oscillation amplitude is larger for smaller ζ (also see Fig. 3). In addition, as $\zeta\to 0$, the characteristic frequency of the oscillations decreases. However, the 1D data in Fig. 4(a) is less clear. In fact, we do not find convincing evidence of periodic oscillations in 1D, but cannot rule out such a possibility just from these data because we could not extend 1D simulations for very small ζ.

In order to study how the oscillations depend on the system size L, we repeated the calculation of the power spectra for several L. In this context we studied mostly $d=2$, where the oscillations are most pronounced. To distinguish the amplitude of periodic oscillations from the statistical noise (which is larger for smaller systems), we estimated the noise

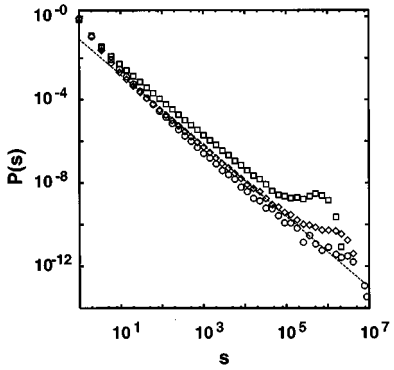

FIG. 6. The distribution of the avalanche sizes $P(s,\zeta\approx 0)$ from $d=1$, 2, and 3 dimensional hypercubic lattices ($\bigcirc$, $\diamond$, and $\square$, respectively). In 1D, $\zeta\approx 0.003\,96$; in 2D, $\zeta\approx 0.001\,70$; and in 3D, $\zeta\approx 0.000\,13$. The dashed line guiding the eye has slope -1.65. These systems had 7–9×10^6 sites depending on the value of d.

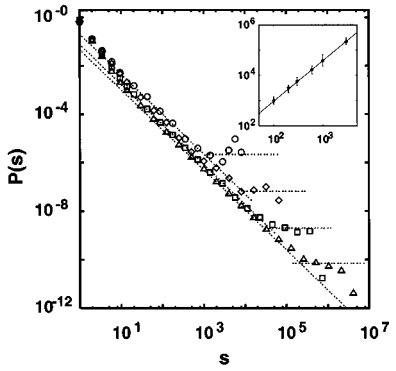

FIG. 7. The 2D distribution of the avalanche sizes $P(s,\zeta\approx 0)$ at $\zeta\approx 0.001\,70$ for various system sizes: $L=100$ ($\bigcirc$), $L=300$ ($\diamond$), $L=1000$ ($\square$), and $L=3000$ ($\triangle$). Diagonal dashed lines have slope 1.65. The inset shows the crossover size $s_{\max}(L)\propto L^{\nu}$, which is estimated from the intercept of dashed lines depicting the power-law decay and plateaulike regime. The solid line in the inset has slope 1.6.

level S_n from the average of the signal S far away from the peak. The scaled spectra $S(\omega)/S_n$ should describe the signal to noise ratio. For example, Fig. 5 displays $S(\omega)/S_n$ for $\zeta=0.09$ using systems with linear sizes $L=512$, 1024, and 2000, where the noise level S_n is the average of $S(\omega)$ between $\omega=0.5$–0.8. We find that the spectra show an oscillatory behavior with $\omega\approx 0.08$, where the frequency does not depend on L. Additionally, the relative amplitude of the oscillations is an increasing function of L. Similar tests with other values of ζ, as well as the 3D data, yielded the same conclusions (data not shown). Thus we conclude that the periodic oscillations in the particle coverages are not due to the finite size effects.

C. Distribution of avalanche sizes

We start this section by testing Eq. (18). For that purpose we have utilized the constant-B coverage ensemble, which facilitates the simulations at small ζ. As discussed above, the lower limit in ζ is set by the available computer memory. Figure 6 shows the calculated $P(s,\zeta\approx 0)$ using the data for smallest ζ available to us. Indeed, the data confirm Eq. (18), apart from deviations for very large s, which are mainly due

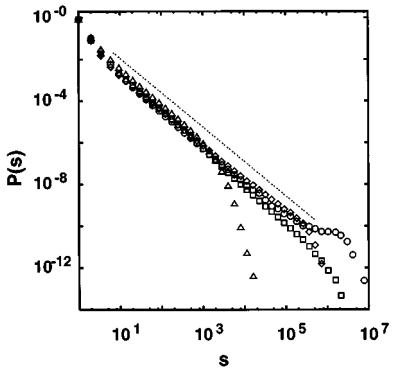

FIG. 8. The 2D distribution of the avalanche sizes $P(s,\zeta)$ for various values of ζ: $\zeta\approx 0.001\,70$ ($\bigcirc$), $\zeta\approx 0.0163$ ($\diamond$), $\zeta=0.05$ ($\square$), and $\zeta=0.09$ ($\triangle$). The dashed line has slope 1.65.

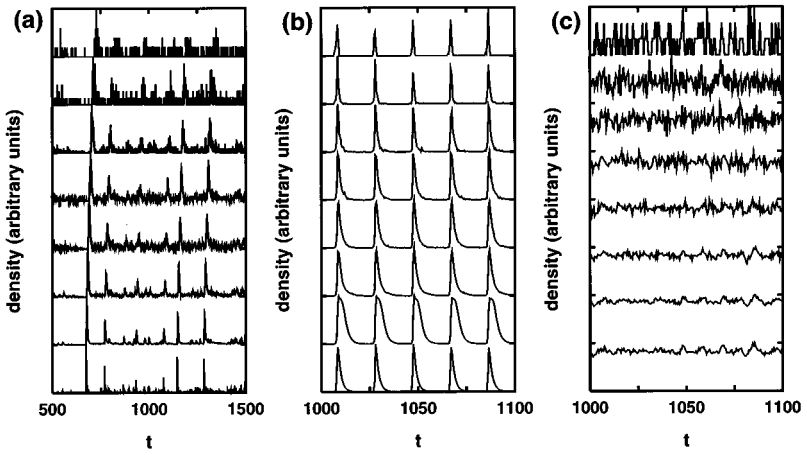

FIG. 9. The time dependence of θ_B and of the number of the avalanches of size s and ρ_s, where ρ_s's are averaged over a bin $[2^{k/2},2^{1/2}2^{k/2}]$. The figures show (from bottom to top) θ_B and ρ_s's with $k=0$, 2, 4, 6, 8, 10, and 12. The data are collected using (a) $\zeta=0.265$ in 1D, (b) $\zeta=0.05$ in 2D, and (c) $\zeta=0.023$ in 3D. For clarity, the number of avalanches, as well as θ_B, is scaled such that the maximum equals unity.

to the finite system size (see below). We estimate that $\tau=1.65\pm0.1$, where τ seems to (but need not) be independent on d.

To study how P depends on the size of the system, we repeated the 2D simulations at $\zeta\approx0.00170(\theta_B=10^{-3})$ for several L. The results are displayed in Fig. 7. From these data it is apparent that for finite systems Eq. (18) holds only up to a size dependent cutoff $s_{\max}(L)$, at which the data levels toward a plateaulike regime. The dashed lines in Fig. 7 illustrate this kind of behavior. We estimated the crossover size $s_{\max}$ roughly from the intercepts of these lines. Plotting the estimates as a function of L, as done in the inset of Fig. 7, indicates that $s_{\max}$ grows algebraically with L,

$$s_{\max}\propto L^{\nu}, \tag{25}$$

where $\nu_{2D}=1.6\pm0.1$.

Figure 8 shows the measured distribution $P(s,\zeta)$ for several values of ζ in 2D. The data show that a nonzero ζ has a similar effect as the finite system size. It introduces a cutoff size to the power-law decay of P. For $\zeta>0$, the data seem to decay roughly exponentially for very large $s>s'_{\max}(\zeta)$, but we have not performed detailed study of the scaling of P or $s'_{\max}(\zeta)$. In conclusion, we find that as $\zeta\rightarrow\zeta_c=0$ the model has avalanches of *all sizes*. Test runs in 2D indicate that either the finite system size or nonzero ζ, does not qualitatively affect the power-law decay until a certain cutoff size.

D. Avalanche density as a function of time

This section deals with the number of the avalanches as a function of time, which has been measured from direct MC simulations. Figure 9 shows θ_B and the number of avalanches of size s, ρ_s, as a function of time. For clarity, $\rho_s(t)$ are calculated by collecting the data over exponentially increasing bins, and the data are scaled such that the maximum equals unity. Especially the 2D data in Fig. 9(b) show that the oscillations in θ_B involve avalanches of *all sizes* (instead of being determined by the largest avalanches, for example). Remarkably, the ρ_s's are also *synchronized* such that they occur with the same characteristic ω for all s.

While the 1D and 3D data are less clear, we calculated the power spectra of ρ_s from the data of Figs. 9(a) and 9(c). The resulting spectra are shown in Fig. 10 together with the $S(\omega)$ of θ_B. Indeed, the spectra indicate that the avalanches in 3D possess similar synchronization as in 2D [see Fig. 10(b)], i.e., all ρ_s show the same characteristic frequency $\omega\approx0.1$. On the other hand, the 1D spectra for ρ_s are practically identical to that of θ_B, but they do not show evidence of periodic oscillations.

VI. DISCUSSION

A. Static aspects

The average coverages, e.g., $\langle\theta_B\rangle$, are reasonably well understood using the implications from the rate equations, especially Eq. (9). We find that near $\zeta_c=0$, $\langle\theta_B\rangle$ (as well as $\langle\theta_A\rangle,\langle\theta_*\rangle$) decay as a power law characterized by an exponent β. At $d=2$ the measured β agrees with the MF result $\beta_{\mathrm{MF}}=0$.

Concerning $P(s,\zeta)$, this autocatalytic reaction model shares many features with forest-fire models [21,22], which have been introduced as possible realization of self-organized criticality [23]. Specifically, we find that $P(s,0)$ decays as a power law up to a finite-size cutoff $s_{\max}\propto L^{\nu}$. However, the current model is rather critical in the usual sense of the word, as one needs to tune $\zeta\rightarrow\zeta_c=0$ to achieve

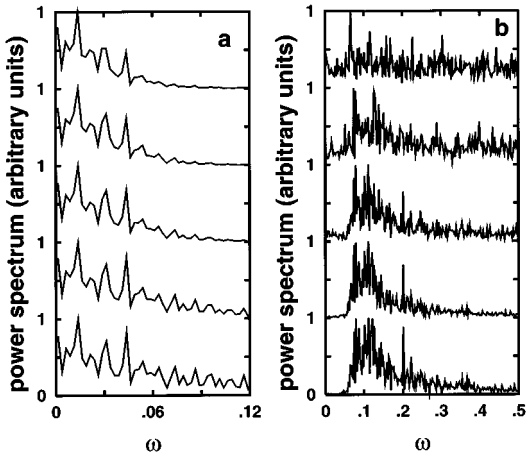

FIG. 10. The power spectra of (a) 1D and (b) 3D data for θ_B and ρ_s's [these data are shown in Figs. 9(a) and 9(c)]. The displayed spectra (from bottom to top) are for θ_B, and ρ_s with $k=0$, 2, 4, and 6. For clarity, the spectra are scaled such that the maximum equals unity.

the critical state. For $\zeta>0$, $P(s,\zeta)$ decays roughly exponentially for $s>s'_{\max}(\zeta)$.

B. Periodic oscillations

The main motivation for studying this particular model is the complicated temporal behavior, involving periodic oscillations in the coverages. The simulation results presented above give evidence that the model exhibits temporal oscillations in the coverages of the adsorbates, at least in two and three dimensions.

We find that these periodic oscillations near $\zeta=0$ are related to synchronized avalanches, which occur with a well defined frequency and come in all possible sizes (i.e., exhibit power-law scaling). Although we do not have a complete theory for the emergence of the oscillations, possibly the simplest heuristic explanation for this synchronization of the avalanches is the following. [Look at Fig. 9(b), for example.] The typical cycle consists of a sudden increase of θ_B followed by a slower decrease. In the end of this decrease period, as most B's have desorbed, θ_B is very small, and A clusters are free to grow. As there are very few $A+B$ reactions, typical A clusters grow until there is a nonzero probability that an arbitrary cluster is separated from a B molecule only by a single vacant perimeter site. This happens as θ_A is close to the critical occupancy $\tilde{p}_c(\theta_B)=p_c(\zeta)$ of this kind of a random deposition problem.

This heuristics should qualitatively account for the observed temporal behavior of this model. Most importantly, the identification with such a deposition problem should be compatible with Eq. (18), because one would reasonably expect that at the critical $\theta_A=p_c(\zeta)$ the surface contains A clusters of all sizes. In addition, during each period the number of A adsorptions $N_{\rm ads}$, which is needed to attain $p_c(\zeta)$ has $N_{\rm ads}\approx\zeta\langle N_*\rangle/\omega$. Thus

$$\begin{aligned} p_c(\zeta)&\approx\max(\theta_A)\approx\min(\theta_A)+N_{\rm ads}L^{-d}\\ &\approx\min(\theta_A)+\frac{\zeta\langle N_*\rangle L^{-d}}{\omega}\\ &=\min(\theta_A)+\frac{\zeta\langle\theta_*\rangle}{\omega}. \end{aligned} \tag{26}$$

Using $\langle\theta_*\rangle\propto\zeta^{\beta}$, we find

$$\omega\approx\zeta^{1+\beta}/[\max(\theta_A)-\min(\theta_A)]. \tag{27}$$

Thus the characteristic frequency of the periodic oscillations is independent of L. As the amplitude of the oscillations, $\frac{1}{2}[\max(\theta_A)-\min(\theta_A)]$, will increase when the average size of the avalanches increases, $\omega\to0$ as $\zeta\to0$, in agreement with the numerical data.

In principle, this heuristic explanation does not make a difference between different dimensionalities. However, it may happen that for some d, $p_c(\zeta)\to1$ for $\zeta\to\zeta_{c,2}>0$, which may cause that direct numerical simulations tend to the poisoned state $\theta_A=1$ already at $\zeta_{c,2}>\zeta_c=0$. It seems to us that this is the case in $d=1$, with $\zeta_{c,2}=0.262\pm0.005$. Thus we believe that the oscillations are not present in one dimension.

VII. CONCLUSION

In conclusion, we have reported analytical and numerical studies for a simple autocatalytic surface reaction model, which consists of two kinds of particles, say, A and B. Particle A adsorbs with rate ζ, particle B desorbs with rate $1-\zeta$, and there is an infinitely fast autocatalytic reaction step $A+B\to2B$ occurring on the surface. In particular, the static aspects of this model, like the behavior of the average coverages as a function of the control parameter ζ, are well understood from simple arguments which use rate equations. Detailed studies of the temporal behavior of this model reveal periodic oscillations in the coverages (near $\zeta_c=0$) for $d=2,3$, but not for a 1D model. Our data show that these periodic oscillations are related to *synchronized* avalanches of $A+B\to2B$ reactions. These avalanches occur with a well defined frequency, and come in *all* possible sizes. We were not able to formulate a complete theory for the emergence of these oscillations, but our heuristic argument, which postulates that the model is driven toward a critical state of a random deposition problem, is qualitatively able to account for the observed temporal behavior of this model in $d\leqslant3$.

ACKNOWLEDGMENTS

This work has been made possible by generous computer resources from the Center of Scientific Computing, Finland. We have benefited from the discussions with Professor H. Park. J.-P.H. gratefully acknowledges financial support from the Neste Foundation and the Finnish Cultural Foundation.

[1] P. Gray and S. K. Scott, *Chemical Oscillations and Instabilities: Non-linear Chemical Kinetics* (Clarendon, Oxford, 1990).
[2] M. M. Slinko and N. I. Jaeger, *Oscillating Heterogeneous Catalytic Systems, Studies in Surface Science and Catalysis 86* (Elsevier, Amsterdam, 1994).
[3] R. Imbihl, M. P. Cox, and G. Ertl, J. Chem. Phys. **84**, 3519 (1986).
[4] R. Imbihl, in *Springer Series in Synergetics*, edited by P. J. Plath (Springer, Berlin, 1989), Vol. 44, pp. 26–64.
[5] J. Lauterbach and H. H. Rotermund, Surf. Sci. **311**, 231 (1994).
[6] Th. Fink, J.-P. Dath, R. Imbihl, and G. Ertl, J. Chem. Phys. **95**, 2109 (1991).
[7] G. Veser and R. Imbihl, J. Chem. Phys. **96**, 7155 (1992).
[8] S. J. Lombardo, Th. Fink, and R. Imbihl, J. Chem. Phys. **98**, 5526 (1993).
[9] B. Kasemo, K.-E. Keck, and T. Högberg, J. Catal. **66**, 441 (1980).
[10] B. Kasemo and K.-E. Keck, Surf. Sci. **167**, 313 (1986).
[11] J. E. Turner, B. C. Sales, and M. B. Maple, Surf. Sci. **103**, 54 (1981).
[12] M. Ehsasi, C. Seidel, H. Ruppender, W. Drachsel, J. H. Block, and K. Christmann, Surf. Sci. **210**, L198 (1989).
[13] M. Ehsasi, O. Frank, and J. H. Block, Chem. Phys. Lett. **165**, 115 (1990).
[14] K. Binder, in *Monte Carlo Methods in Statistical Physics*, ed-

ited by K. Binder, Topics in Current Physics Vol. 7 (Springer, Berlin, 1986), p. 1.
[15] J. Honerkamp, *Stochastische Dynamische Systeme* (VCH, Weinheim, 1990).
[16] A. P. J. Jansen, Comput. Phys. Commun. **86**, 1 (1995).
[17] J. Mai, V. N. Kuzovkov, and W. von Niessen (unpublished).
[18] J. Mai, V. N. Kuzovkov, and W. von Niessen, J. Chem. Phys. **100**, 6073 (1994).
[19] R. M. Ziff and B. J. Brosilow, Phys. Rev. A **46**, 4630 (1996).
[20] R. M. Nieminen and A. P. J. Jansen, Appl. Catal. (to be published).
[21] J. E. S. Socolar, G. Grinstein, and C. Jayaprakash, Phys. Rev. E **47**, 2366 (1993).
[22] B. Drossel, Phys. Rev. Lett. **76**, 936 (1996), and references therein.
[23] P. Bak, C. Tang, and K. Wiesenfeld, Phys. Rev. Lett. **59**, 381 (1987); Phys. Rev. A **38**, 364 (1988).